Tellus (1995), 47A, 766–778
Printed in Belgium – all rights reserved

TELLUS
ISSN 0280–6495

Coupled ocean wave/atmosphere mesoscale model simulations of cyclogenesis

By JAMES D. DOYLE, *Marine Meteorology Division, Naval Research Laboratory, 7 Grace Hopper Ave., Monterey, CA 93943-5502, USA*

(Manuscript received 2 August 1994; in final form 15 February 1995)

ABSTRACT

The impact of wind-generated ocean waves upon the structure and evolution of an idealized cyclone is investigated. High-resolution numerical experiments were performed with a constant surface roughness, roughness length from Charnock's formula, and from a coupled ocean-wave/atmosphere mesoscale model. Results indicate that young ocean waves increase the effective surface roughness, increase the surface stress, significantly decrease the 10-m wind speeds and modulate the heat and moisture transport between the atmosphere and ocean. These effects are maximized along the warm front and to the rear of the cyclone near the southwestern quadrant. As a result of this boundary layer modification, the mesoscale structures associated with the cyclone are perturbed. Regions of young windsea act to locally enhance the low-level frontogenesis, convergence and rainfall. Roughness effects associated with ocean waves modulate the deepening rate during rapid cyclogenesis and enhance the cyclone filling process. Kinetic energy of the entire cyclone system is reduced significantly near the surface and by 3–8% above the boundary layer as a result of enhanced roughness associated with young ocean waves.

1. Introduction

The interaction of the ocean and atmosphere has long been recognized as an important element of marine cyclogenesis. It is well documented that explosive cyclones frequently occur in winter near strong sea-surface temperature (SST) gradients (Sanders and Gyakum, 1980). Early studies hypothesized that sensible and latent heat fluxes were important for modification of cold-air streams over the North Atlantic and subsequent influence on cyclogenesis (Brunt, 1930; Pettersen et al., 1962). More recently, numerous observational (Bosart, 1981; Neiman and Shapiro, 1993) and model-based sensitivity studies (Danard and Ellenton, 1980; Kuo et al., 1991; Doyle and Warner, 1993) have documented a wide range of impacts of surface heat and moisture fluxes upon the development and structure of marine cyclones. These studies suggest that the structure and dynamics of oceanic cyclones may be significantly modulated by the heat and moisture exchange between the ocean surface and the atmosphere.

Numerous studies also have shown that frictional dissipation during cyclogenesis can be significant. Early numerical studies by Graystone (1962) and Danard (1969) noted substantially weaker cyclones in the presence of surface friction. Anthes and Keyser (1979) found that the removal of surface friction from a 24-h numerical simulation of a continental cyclone resulted in a central pressure that was 33 mb deeper. In spite of the weaker intensity, the frictional convergence resulted in greater rainfall rates. In a numerical study of explosive cyclogenesis over the Pacific Ocean, Kuo and Reed (1988) found that in the absence of surface friction, the simulated cyclone deepened an additional 5–7 mb. Juang and Ogura (1990) noted that large surface-layer friction contributed to the erroneously slow development and merging of two continental cyclones. The idealized numerical simulations of Hines and Mechoso (1993) indicate that the surface frontal structure during cyclogenesis is very sensitive to relatively large changes in the surface drag coefficient. In these adiabatic simulations, an increase in surface drag inhibited warm frontogenesis by decreasing the low-level wind speed and warm advection. Bent-back warm fronts develop in the simulations when small surface drag coefficients (typical of a calm ocean surface) are used, however are absent in simulations that use coefficients representative of land surfaces.

Despite the importance of frictional dissipation during the life cycle of a continental cyclone, the impact of the exchange of momentum between the ocean surface, due to wind-driven waves, and the marine atmospheric boundary layer (MABL) has received considerably less attention. Recent studies by Janssen et al. (1989) and Janssen (1991) suggest that the effect of wind-generated ocean waves can have an important influence upon the wind stress in the surface layer because the wave-induced stress is a considerable fraction of the total stress (Komen, 1985). Thus, the MABL response to rapid cyclogenesis, as well as the mesoscale and synoptic-scale cyclone structure, may be modulated by wind-generated ocean waves. Ulbrich et al. (1993) found that increased surface roughness in the Southern Hemisphere storm track significantly modified the tropospheric circulation including a reduction of 10% in the tropospheric winds near the storm track. The results of Janssen et al. (1989) and Nordeng (1991) suggest that a coupled ocean wave-atmospheric modeling system may be required to properly parameterize the interface between the ocean and atmosphere. Following this approach, Weber et al. (1993) and Janssen (1994) coupled a general circulation model to the Wave Model (WAM) (WAMDI Group, 1988) and found varying impacts on the large-scale circulation and storm track. However, the impact of ocean waves upon the mesoscale and synoptic-scale structure of marine cyclones has not been addressed.

In this investigation, the interaction between ocean waves and the MABL during coastal cyclogenesis is examined using a coupled mesoscale-ocean wave modeling system. This study represents the first time a fully predictive ocean wave model is coupled in a two-way interactive manner to a mesoscale model with sophisticated boundary-layer and precipitation parameterization schemes. This two-way interaction enables information to be passed between the wave and atmospheric models during the simulation. The specific objectives are to: (1) use the coupled-model generated dataset to analyze the response of the boundary-layer, mesoscale and synoptic-scale environment associated with marine cyclogenesis to the oceanic sea state; (2) evaluate the performance of the Charnock (1955) roughness parameterization, which is commonly used in mesoscale models, during explosive cyclogenesis; (3) provide a test for the ocean wave-atmosphere coupling theory of Janssen et al. (1989) in an optimal model environment with very high resolution in space and time. The specific focus of this study will be upon the air-sea interaction during the rapid development stage of the cyclogenesis. For simplicity, an idealized cyclone is simulated in this study. Thus, it is not possible to assess changes in the predictive skill of cyclogenesis that may be associated with the coupled-modeling system. Nevertheless, as an important first step, the results establish the sensitivity of marine cyclogenesis to ocean-wave induced frictional enhancement of the surface stress. The coupled model and experimental design are described in Section 2. The model results are presented in Section 3. The summary and conclusions are provided in Section 4.

2. Model and experimental design

The atmospheric model used in this study is the Navy's Coupled Ocean Atmospheric Mesoscale Prediction System (COAMPS). The three-dimensional model solves the fully compressible equations of motion on an f-plane. Physical parameterizations include a convective parameterization scheme with parameterized subgrid-scale downdrafts (Kain and Fritsch, 1990), explicit moist physics with ice parameterization (Rutledge and Hobbs, 1983) and a level 2.5 subgrid-scale planetary boundary-layer parameterization scheme with a predicted turbulent kinetic energy (TKE) budget (Therry and Lacarrére, 1983). A complete model description of COAMPS can be found in Hodur (1993). In the standard COAMPS, in the absence of a coupled predictive ocean-wave model, the roughness length, z_o, is computed over the open sea by Charnock's relation (Charnock, 1955)

$$z_o = \alpha \frac{\tau}{g\rho}, \tag{1}$$

where τ is the magnitude of the turbulent stress, ρ is the density, g is the gravitational constant, and

α is the Charnock constant taken to be 0.0185. For small low-level wind speeds, z_o is set to 0.02 cm.

The atmospheric model is coupled in an interactive mode to the 3rd generation (cycle 4) of the WAM (WAMDI Group, 1988) using the quasi-linear theory of wind-wave generation following Janssen et al. (1989) and Janssen (1991). In the WAM model, the transport equation is integrated to solve for the wave variance spectrum for 25 frequencies and 24 directions. The wave model simulates the generation of wind-driven ocean waves, the transfer of energy within the wave spectrum, wave propagation, and dissipation by whitecapping. The wave-induced stress is defined as the integral over all directions and spectral components of the atmospheric momentum flux to the wind-generated wave field (Janssen, 1989). The total atmospheric stress consists of contributions from flow over a rigid flat surface and wind-generated wave. When the wave field is dominated by a young windsea, which occurs during the initial stage of wave growth, the wave-induced stress is large. An increase in the wind speed or a change in wind direction are typically associated with wave growth and a young windsea. As waves grow, the total energy of the wave field increases and the energy containing range of the frequency spectrum shifts toward lower frequencies until an equilibrium is achieved between the wind and wave field. The WAM is a widely used model and forecast wave heights have been verified extensively against a number of data platforms by numerous investigators. These studies show that with a reliable specification of the wind field, the significant wave height is predicted with a great deal of accuracy.

The method used to couple the models in these simulations is based on the method of Janssen et al. (1989), which includes mutual interaction between the boundary-layer stress and the wind-generated waves. This parameterization incorporates effects of a mixed wind sea, which includes potentially important sea swells. The roughness length used in the coupled simulations is given by

$$z_o = \beta \frac{\tau}{g\rho(1 - \tau_w/\tau)^{1/2}}, \tag{2}$$

where τ is the total stress and τ_w is the wave-induced stress. Here, β has been chosen as 0.010 so that (2) reduces to the standard Charnock formulation (1) (with Charnock constant of 0.0185) for an old windsea. In this application, the roughness length can be enhanced by up to a factor of five, and more commonly by a factor of 2–3, for an extremely young sea. Every 4 atmospheric-model time steps (6 min) the atmospheric stress is communicated to the wave model. With the predicted τ_w and wind speed, the drag coefficient, c_D, and τ are solved iteratively. The stress ratio, τ_w/τ, and the atmospheric stress, τ, computed from the surface-layer parameterization of Louis et al. (1982), are then used to compute the new ocean wave dependent z_o. This method of coupled wind-wave growth yields results that are in agreement with observations of air-flow over wind-generated waves (Smith et al., 1992). Janssen (1991) used an assumed directional distribution and measured wind speed and frequency spectrum from HEXMAX to determine the surface stress from quasi-linear theory. Very good agreement was found between observed and modeled stresses, which provides confidence in the coupled modeling system.

The atmospheric model has a total of 32 vertical levels, with greater resolution in the lower troposphere (13 levels below 850 mb) to enable a good representation of the interaction of the wave-induced stress within the MABL and lower-tropospheric processes. The model grids for the ocean wave and atmospheric modules contain 133x133 points with a horizontal grid increment of 30 km. The model is used in a channel mode with periodic boundary conditions in the zonal direction for both the wave and atmospheric predictive variables. A time step of 90 s is used for the atmospheric model and 6 min for the ocean wave model. All simulations are integrated to 96 h, which enables the rapid development and early decay phases of the idealized cyclone to be studied. A coupled simulation with both the wave and atmospheric models requires approximately 11% more CPU time than an uncoupled atmospheric simulation.

The initial conditions consist of a zonally symmetric jet stream based on winter-mean conditions (Oort, 1983). The maximum wind speed is 80 m s^{-1} near the center of the domain at approximately 11 km (250 mb). The wind is assumed to be near zero at the surface. The initial temperature distribution is found from thermal wind balance and a temperature profile based upon the standard atmospheric lapse rate. A small longitudinal wind component below 250 mb, specified as a sinusoidal function that damps near the boundaries, is used to provide the initial perturbation for the baroclinically unstable jet. The initial moisture field is based on climatology as well (Lorenz, 1967). Two different idealized SST patterns are specified and held constant during the simulations. In one set of experiments, a zonally oriented SST pattern centered beneath the axis of the jet stream is used. Values of the SST gradient ($3°C\ (100\ km)^{-1}$) and temperature difference between the warm and cold sides of the idealized current (18°C) are in agreement with climatological values for the Gulf Stream and the Kuroshio Current. In a second set of experiments designed to test the sensitivity to a different SST distribution and resulting surface forcing, a sinusoidal SST structure following Nuss and Anthes (1987) is used.

In order to examine the impact of the interactions between the ocean waves and atmospheric boundary layer, three sets of three numerical experiments were performed. The first experiment (ZSST) makes use of the zonal SSTs and a constant roughness length of 0.02 cm. The identical simulation with a Charnock's relation for roughness following (1) is used in CHZSST. The fully coupled ocean wave-atmospheric model simulation with the zonal SSTs are used in COZSST. Similar experiments are performed with the sinusoidal or wave-like SST and are denoted as WSST (constant z_o), CHWSST (z_o from Charnock's relation), and COWSST (wave stress from the WAM), respectively. The third set of experiments, NSF (constant z_o), CHNSF (z_o from Charnock's relation), and CONSF (wave stress from the WAM) have no surface heat or moisture fluxes, however surface momentum fluxes are included.

3. Results

3.1. MABL response

The simulated 60-h sea-level pressure is shown in Figs. 1a–c for ZSST, CHZSST, and COZSST, respectively. At this time the simulated cyclone is located near the eastern portion of the domain and has deepened substantially in all three simulations. The near-surface wind speeds (wind speeds in excess of $25\ m\ s^{-1}$ shown in Fig. 1) are strongest in the southwestern quadrant of the cyclone and to the north of the warm front extending westward along the bent-back warm front. Not surprisingly, ZSST, the simulation that used a small constant roughness length (0.02 cm), which approximates viscous flow over a ocean surface void of waves, produced maximum 10-m wind speeds ($35.2\ m\ s^{-1}$) that were 12% greater than for CHZSST ($31.3\ m\ s^{-1}$). The maximum 10-m wind speed ($27.5\ m\ s^{-1}$) in the coupled simulation, COZSST, is over 20% weaker than for ZSST and 12% weaker than CHZSST. The differences among the three simulations in the maximum 10-m wind speed are quite variable. In general, the wind speeds are most different among the simulations during rapid cyclogenesis phase (between 48 and 60-h), with the coupled simulation having the weakest winds. Root-mean-squared (RMS) 10-m wind vector differences during the rapid development phase between the coupled experiment and the CHZSST and ZSST simulations, computed over the entire domain, are between $1.8\ m\ s^{-1}$ and $4.4\ m\ s^{-1}$.

The high wind speeds in the COZSST simulation result in the substantial growth of surface ocean waves. A frequently used parameter to describe the ocean wave field is the significant wave height, H_s, which is equivalent to the average height of the highest one-third of the ocean waves, or $H_s = 4(E)^{0.5}$, where E is the wave variance. The growth of ocean waves is influenced by wind velocity, fetch and duration. Often, large significant wave heights are observed in the open ocean, however, for offshore flow in the coastal zone, wave heights are limited because of the finite fetch. The 60-h H_s field for COZSST, shown in Fig. 2, indicates that significant wave heights are in excess of 12 m in the southwestern quadrant of the cyclone. The wave height maximum is located 240 km upstream of the maximum 10-m wind speeds. A secondary maximum of 6 m is located to the northeast of the surface cyclone and slightly downstream of a secondary 10-m wind speed maximum positioned to the north of the warm front. The two local wave height maxima are linked spatially and temporally to the local 10-m wind speed maxima (Fig. 1) in agreement with the simulations of Weber et al. (1993). These wave heights are similar to values observed during rapid coastal cyclogenesis (Dolan and Davis, 1992).

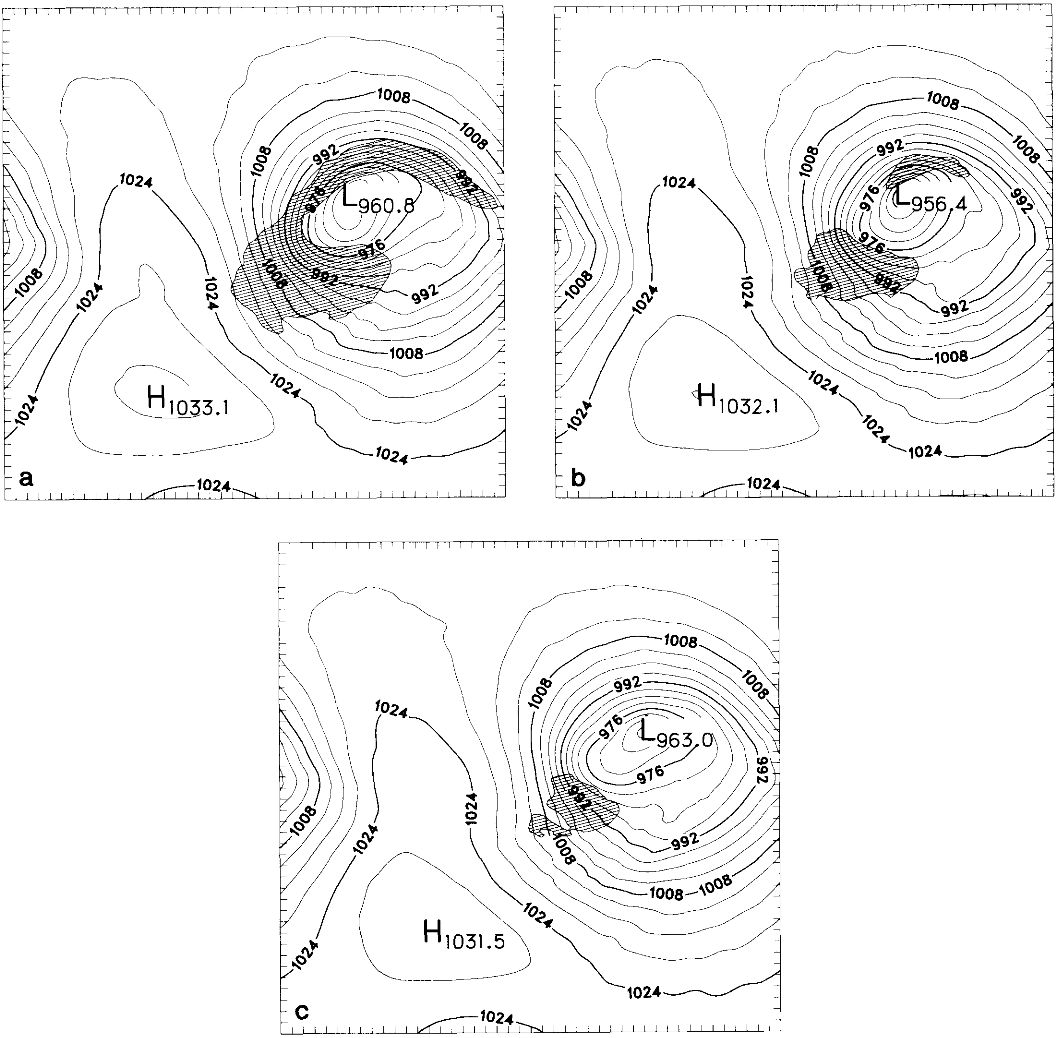

Fig. 1. Simulated sea-level pressure for the (a) ZSST, (b) CHZSST, and (c) COZSST simulations for the 60-h time. The isopleth interval is 4 mb. Regions of 10-m wind speeds in excess of 25 m s^{-1} are denoted by the shading. Tick marks are plotted along the borders every third grid point or 90 km.

The regions where the stress ratio (τ_w/τ) is greater than 0.9 are shaded in Fig. 2. The stress ratio is an indicator of the strength of coupling between the waves and the MABL (Janssen, 1991; Weber et al., 1993). In these shaded regions, ocean wave-MABL coupling is high as a result of relatively young (growing) waves. It follows from (2) that this young windsea region results in an increase by a factor of three or more in z_o compared with the z_o obtained from Charnock's relation (1). The difference between the 60-h roughness length fields for CHZSST and COZSST are shown in Fig. 3. In a few isolated regions in the southwestern quadrant of the cyclone and along the warm front, the roughness length in the coupled simulation is over 1 cm greater (increase by more than a factor of five) than that of the CHZSST simulation. Numerous observational

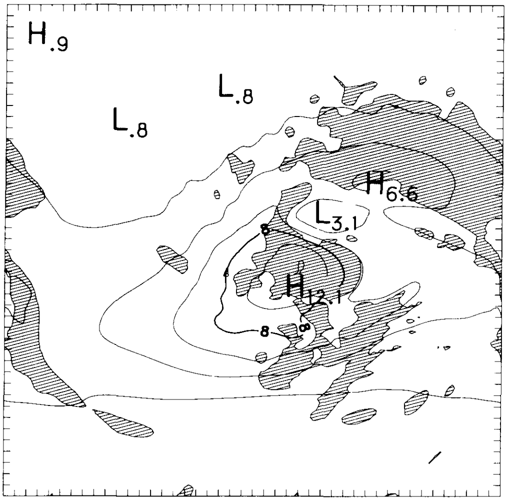

Fig. 2. Simulated significant wave height (m) for the 60-h time for COZSST. The isopleth interval is 2 m. Regions of stress ratio (τ_w/τ) greater than 0.9 are denoted by the shading.

studies have noted rougher waves after a frontal passage. It has also been shown that boundary-layer momentum is transferred to young, growing waves, while fully-developed waves travel faster than the wind due to transfer of energy to lower frequency and longer wavelength. These fully developed waves do not contribute to an increase in the effective roughness. Thus, in regions of rapidly changing winds, such as near fronts, a young windsea will prevail and the ocean wave-MABL coupling will be large. Additionally, during the rapid development phase, the near-surface ageostrophic winds are increasing rapidly in response to the changing pressure field. As a result, young or growing waves are prevalent, especially along the warm front and in the southwestern quadrant. In the large-scale simulations of Weber et al. (1993), the stress ratio was enhanced in the vicinity of cyclones, particularly in the frontal zones.

The relationship between the simulated wave-age parameter, C_p/u_*, where C_p is the phase speed of the peak spectral frequency and u_* is the friction velocity, and the dimensionless roughness length (gz_o/u_*) for the 60-h time is shown in Fig. 4. Every 5th grid point from the coupled model are plotted for values where $C_p/u_* < 25$, which corresponds to a young-wind sea. Regression fits based on observational data from Smith et al. (1992) taken during HEXOS, shown in Fig. 4, indicate a good agreement between the observations and simulated wave age and Charnock parameters, as also discussed in the coupled modeling work of Janssen (1994). The simulations that make use of the use of the Charnock formula (1) (i.e., CHZSST, CHWSST and CHNSF) have dimensionless

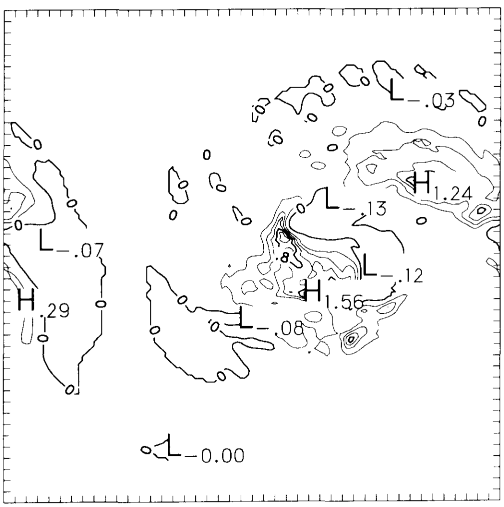

Fig. 3. Roughness length difference field $(10^{-2}\,\mathrm{m})$ between CHZSST and COZSST for the 60-h time. The isopleth interval is 0.2×10^{-2} m.

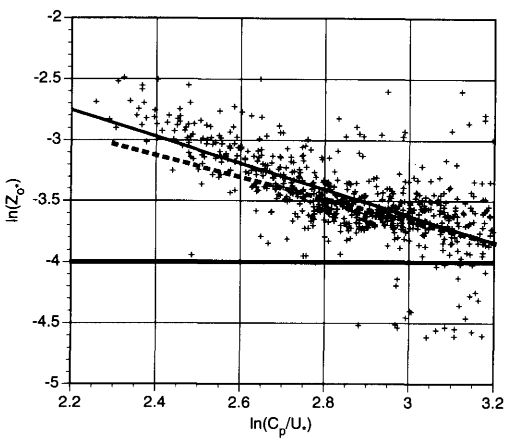

Fig. 4. Simulated dimensionless roughness length $z_{o*} = gz_o/u_*^2$ as a function of the wave-age parameter for the 60-h time for COZSST. The Charnock formula with a constant of $\beta = 0.0185$ is shown by the solid line at $\ln(z_{o*}) = -4.0$. The dashed line represents the Smith et al. (1992) best fit.

roughness lengths of -4.0 (corresponding to $\alpha = 0.0185$). For fully saturated and oversaturated waves ($C_p/u_* > 25$) the Charnock formula appears to be sufficiently accurate (Maat et al., 1991). However, for a relatively young windsea ($5 > C_p/u_* < 25$), use of the Charnock formula significantly underestimates the dimensionless roughness length. Thus, differences that develop between the simulations that use the Charnock formula and the coupled simulations can be attributed to roughness effects associated with young ocean waves.

Despite the relatively large increase in z_o as a result of the ocean wave-MABL interaction, the surface momentum flux and friction velocity change only a modest amount. In a neutrally stratified boundary layer, the neutral drag coefficient, C_{Dn}, can be expressed as

$$C_{Dn} = \left(\frac{0.4}{\ln(z/z_o)}\right)^2. \tag{3}$$

Thus, a relatively large change in z_o results in only a moderate change in the neutral drag coefficient. For example, an increase in the z_o from 0.5 cm to 1.25 cm, only results in a 29% increase in the 10-m C_{Dn}. The surface stress correspondingly increases by a similar amount. Additionally, the larger momentum flux that is present in the coupled simulation acts to reduce the boundary-layer wind speeds by several m s^{-1}, which results in a further reduction in the surface stress. Because of these effects, in some areas the surface stress is smaller in COZSST than in CHZSST, despite the larger z_o in COZSST. Nevertheless, the local maximum momentum flux averaged over the period of rapid deepening (between 48 and 60 h), is 15% and 200% larger in COZSST than in CHZSST and ZSST, respectively. The RMS momentum flux difference between the coupled model simulation and the CHZSST and ZSST simulations, averaged over the same time period, is 0.13 N m^{-2} and 0.19 N m^{-2}, respectively. In localized regions where MABL stratification is stable and the boundary layer becomes somewhat decoupled from the surface below, such as to the north of the warm front, the impact of the z_o increase is much less.

Scatter plots of the simulated drag coefficients (not shown) indicate differences of up to 50–60% exist between the CHZSST and COZSST experiments. A large amount of scatter for the CHZSST simulation results from boundary-layer stability influences, while in COZSST, both stability and wave-age effects contribute to an even greater variability. Janssen (1994) also found substantial differences between the drag coefficient determined by the Charnock formula and a two-way coupled model. The drag coefficients for the coupled model for these simulations are in general agreement with observed (Smith et al., 1992) and modeled drag coefficients (Janssen, 1991; Janssen, 1994). This agreement is not surprising since the observed drag coefficients have been previously used in the development of the coupling technique.

As a consequence of the changes in the friction velocity that occur as a result of the two-way ocean wave-MABL interactions, considerable variability is present in the simulated surface sensible heat and moisture fluxes. The largest differences in these simulations are located in the region where cold air is flowing southward over warm SSTs to the rear of the cyclone. As a result of the young windsea, the larger z_o in COZSST to the southwest of the surface cyclone (Fig. 3) contributes to a larger friction velocity in COZSST than in ZSST and CHZSST. It follows that the maximum surface sensible heat flux at 60 h in the southwestern quadrant is 16% and 60% larger in COZSST than in CHZSST and ZSST, respectively. The RMS surface heat flux difference over the entire domain between the coupled model simulation and CHZSST and ZSST, averaged over the rapid development phase, is 26.8 W m^{-2} and 39.5 W m^{-2}, respectively. Comparable differences are present in the moisture fluxes as well. Similar results are found in the simulations using the sinusoidal SST pattern. For example, the 60-h maximum surface sensible heat flux in COWSST is 59% larger than WSST and 31% larger than CHWSST. Observations have not indicated a clear relationship between the fluxes of heat and moisture and the wave state that would support these differences. However, Janssen (1994) compared the Stanton number and the drag coefficients from the coupled model and found good agreement with observational data. In this mesoscale application, the Stanton number is basically independent of the wind speed or sea state in agreement with Janssen (1994). Thus, the momentum transfer appears to be more sensitive to the sea state than the heat and moisture fluxes. However, the simulated differences in the cyclone between CHZSST, ZSST and COZSST may result, in part, from influences of the heat and moisture fluxes, as well as the more dominant momentum fluxes.

The increased surface sensible heating in COZSST that results from enhanced drag due to the presence of wind-generated ocean waves, modulates the local boundary layer structure. In the southwestern quadrant of the cyclone, large drag due to the ocean waves acts to slightly increase mean boundary layer temperature and moisture due to the larger heat and moisture fluxes. In addition to a slight increase in the buoyancy flux, the enhanced momentum flux associated with the ocean waves contribute to an increase in the turbulent kinetic energy (TKE), especially in the southwestern quadrant of the cyclone. For example, the 60-h TKE averaged over a box 480-km on each side located in southwestern quadrant is as much as 20–50% larger in the boundary layer in the coupled simulation than in CHZSST and ZSST. As a result of the increase in TKE, the eddy mixing coefficients for heat and momentum are increased and more heat and moisture is transported upward, which in turn has an impact on the mesoscale environment of the cyclone. Enhanced values of TKE are present in the coupled simulation at other times as well. Similar increases in the eddy mixing coefficients are found in the COWSST simulation compared with WSST and CHWSST. In *localized* regions to the north of the warm front, the statically stable boundary layer is decoupled from the ocean surface and the ocean waves have somewhat less of an impact on the boundary layer structure, despite the large z_0 in COZSST (Fig. 3).

The results from the experiments that had no surface fluxes of heat or moisture, NSF, CHNSF and COZNSF, indicate that the wave-induced stress from wind-driven ocean waves, without any nonlinear interactions with the heat and moisture fluxes, have an important effect on the boundary layer. In these simulations, momentum mixing is reduced and the maximum 10-m wind speeds are several m s^{-1} less than the full physics experiments. As a result of weaker winds, the boundary-layer is less responsive to ocean-wave growth than the full physics simulation, especially in the southwestern quadrant of the cyclone where the interaction of the fluxes of heat and moisture have an important impact on MABL in the full physics simulation. However, along the warm front, the roughness length and momentum flux increase substantially as a consequence of the large wave-induced stress, similar to the full physics experiments. In this region, the surface heat fluxes in the full physics experiments were upward and relatively small or were downward.

3.2. *Cyclone-scale and mesoscale response*

The time evolution of the central pressure of the cyclone for the nine simulations are shown in Figs. 5a–c. The minimum pressure at the initial time is 1010 mb for all simulations. For the first 36 h of the simulations, the cyclone and 10-m wind speeds are weak. As a result, ocean wave growth is minimal and the central pressure of the cyclone varies little among the nine simulations. From Fig. 5, it is apparent that considerable variability exists in the deepening rate among the nine simulations after 36 h. At times, the central pressures are nearly identical, while just several hours later differ by more than 10 mb. The response of the central pressure of the cyclone to frictional changes associated with ocean waves is complex. For example, for the zonal SSTs, the slowest deepening takes place in ZSST, while the comparable experiment with the sinusoidal SSTs, WSST, results in the most rapid deepening rate. This marked variability is undoubtedly influenced by the highly nonlinear interactions between the boundary layer frictional influences, the ocean wave growth and the surface heat and moisture fluxes. Results from the set of experiments identical to the ZSST simulations except without surface heat and moisture fluxes (Fig. 5c), indicate that at times over a 10-mb difference in the minimum central pressure exist between the simulation with constant roughness length (NSF) and the coupled simulation (CONSF). In general, the differences between CHNSF and CONSF in the central pressure of the cyclone are 1–4 mb. These results suggest that the central pressure of the cyclone is sensitive to the fluxes of momentum, as well as heat and moisture, at the air-sea interface. It is noteworthy that after 96 h the coupled simulation has a central pressure that is nearly 4 mb higher than the CHNSF and 5 mb higher than NSF. In general, during the filling stage of the cyclone evolution, the coupled simulations have cyclone central pressures that are higher than the simulations that used the Charnock formula. This

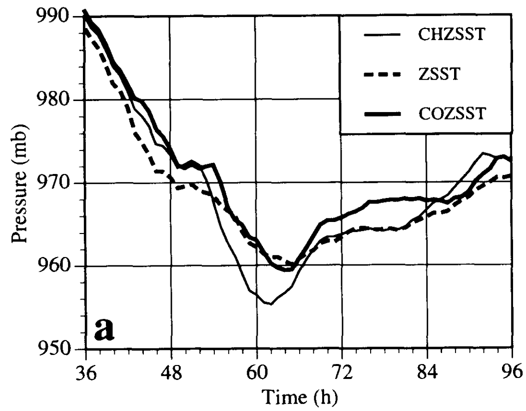

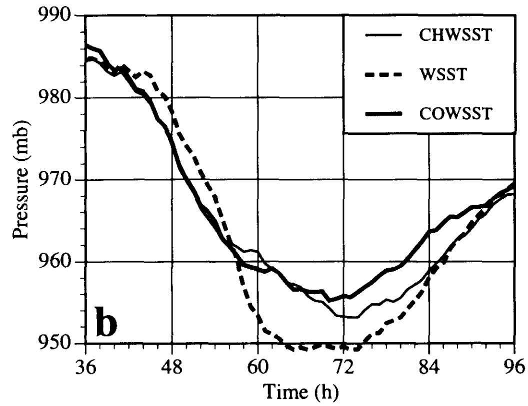

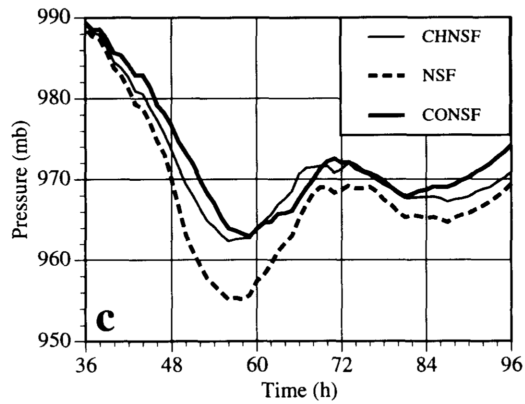

Fig. 5. The central pressure trace of the cyclone for the (a) zonal SST simulations, (b) sinusoidal SST simulations, and (c) no surface heat and moisture flux simulations.

suggests that enhanced frictional stress associated with young ocean waves may augment the filling of marine cyclones, which current operational models typically underforecast (Smith and Mullen, 1993; Harr et al., 1992). Results from simulations performed for an idealized weak development case (maximum deepening rate ≈ 4 mb/12 h) indicate that the cyclone central pressure is relatively insensitive to the roughness effects of ocean waves.

Experiments were performed that were analogous to CHZSST and COZSST and integrated to 48 h. After 48 h, the roughness length in COZSST was computed from (1), identical to that in CHZSST. The results indicate that the differences in the central pressures of the simulations result from local (in space and time) influences of the surface friction rather than perturbed conditions of the pre-cyclogenesis state. This result is not surprising because the major contribution of the wave stress is due to high-frequency waves which respond quickly to changes in wind speed and direction (Janssen, 1989). Weber (1994) used a large-scale general circulation model to show that a large portion of the wave effects on the air-sea fluxes can be described simply by the local and instantaneous wind.

As a result of the transfer of momentum from the MABL to the ocean, the kinetic energy of the cyclone is modified as well. The domain averaged kinetic energy as a result of the roughness impact of the ocean waves is decreased, in agreement with the large-scale simulations of Ulbrich et al. (1993). The greatest fractional decrease in the kinetic energy of the cyclone is confined to the lower troposphere. However, 3–8% differences in the kinetic energy are present up to 400 mb, just below the jet level. Local changes in the kinetic energy are substantially greater than the domain average and indicate that the mesoscale structures differ significantly at times among the simulations, especially in regions where the waves are young near the warm front and in particular to the rear of the cyclone.

The mesoscale structures that develop in the vicinity of the idealized cyclone appear to be sensitive to the roughness effects driven by surface ocean waves. Diagnostic calculations indicate that the roughness changes have a modest impact on the boundary-layer frontogenesis. An example of this impact is shown for a portion of the computational domain for the 60-h zonal SST experiments in Fig. 6. The 900-mb thermal structure is considerably weaker in CHZSST along the warm front than in COZSST. The potential temperature gradient to the east of the cyclone is nearly twice as strong in COZSST than in CHZSST, despite a considerably weakened cyclone in COZSST compared with CHZSST. The region of strong frontogenetic forcing due to horizontal deformation (shaded area in Fig. 6) extends considerably further westward in COZSST than in CHZSST. These differences in the frontal structures are undoubtedly a result of the substantially larger roughness lengths in the vicinity of the warm front (Fig. 3). Differential roughness forcing due to the young windsea leads to more rapid frontogenesis, analogous to a coastline (Doyle and Warner, 1993), though considerably weaker. As a result of the differences in the frontal intensity, the local circulation and thermal advection are modulated in this region as well. At other times and in other experiments (such as the sinusoid SST experiments), local differences of moderate magnitude in the cold and warm frontal strengths exist between the coupled and uncoupled experiments.

Changes in the low-level wind field as a result of ocean wave-induced frictional stress have an important impact on derived low-level quantities such as the divergence, vorticity, and the thermal and vorticity advections, especially along the warm front and in the southwestern quadrant of the cyclone where the heat, moisture and momentum fluxes are large. In these regions, the ocean wave enhanced stress at times appears to maximize the localized regions of convergence and warm advection along the warm front. For example, at the 60-h time the convergence and thermal advection near the warm front just to the northeast of the cyclone is approximately 30% and 10% larger, respectively, in localized regions in COZSST than in ZSST and CHZSST. Additionally, the mesoscale pressure gradient near the center of the cyclone is sensitive to changes in the roughness length as well. For example, at the 60-h time the coupled simulation (Fig. 1c) has a well-defined

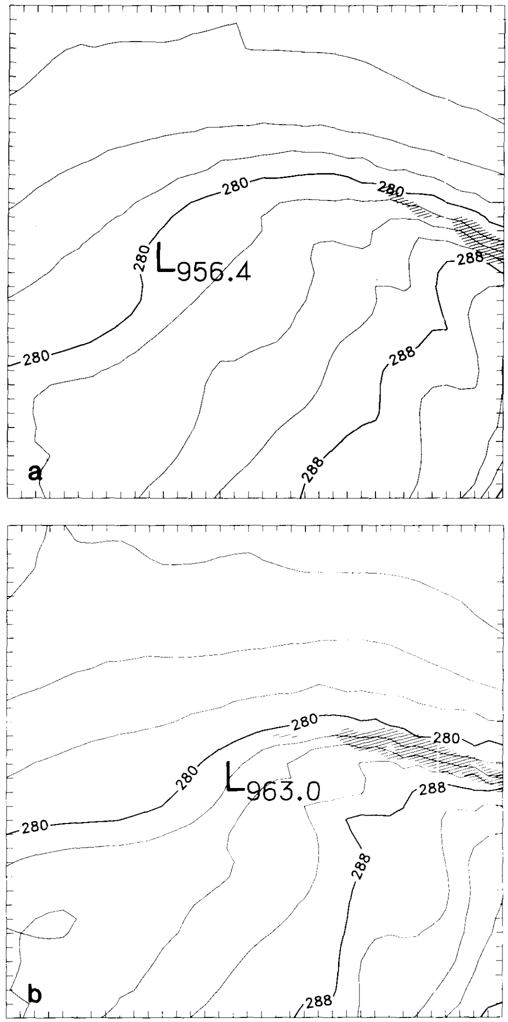

Fig. 6. The 900-mb potential temperature for the 60-h time for (a) CHZSST and (b) COZSST. The isopleth interval is 2 K. Regions of frontogenesis function due to the horizontal deformation greater than 24 K (100 km 6 h)$^{-1}$ are denoted by the shading. For display purposes, only a subsection of the domain is shown. Tick marks are plotted along the borders every grid point or 30 km.

surface pressure trough and weakness in the pressure gradient to the rear of the cyclone, while CHZSST and ZSST (Figs. 1a–b) have considerably different structures. Some of these differences may arise simply from differences in the strength of cyclone.

The variability of the simulated rainfall among the experiments is another indication that the mesoscale structure of the cyclone is sensitive to ocean wave growth. The 12-h accumulated rainfall fields for the 60-h time (not shown) indicate that substantial differences in the accumulated rainfall exist among the ZSST, CHZSST and COZSST simulations along the warm front and in the southwestern quadrant of the cyclone. Once again, in these areas, the stress ratio suggests the presence of young (growing) waves (Fig. 2). The simulated rainfall in the southwestern quadrant appears to be especially sensitive to the roughness effects of ocean waves. In this region, the rainfall maximum is increased by twofold in COZSST compared with ZSST and by 34% relative to CHZSST. The increased fluxes of heat and moisture as a result of the young windsea contribute to more rapid destabilization and moistening of the cold and dry air mass to the rear of the cyclone. As a result of the larger TKE in this region, heat and moisture are mixed through a deeper layer and more vigorously. This destabilization and moistening increase both the grid-scale and subgrid-scale precipitation rates during the rapid development phase. The increase in precipitation in the southwestern quadrant of the cyclone between the coupled and uncoupled simulations is also present for the sinusoidal SST experiments. Along the warm front, the differences among the simulations in accumulated precipitation is complex. In some regions, the roughness enhancement associated with surface ocean waves act to increase the precipitation, while in other regions the simulated precipitation is decreased.

4. Summary and conclusions

In this study, the impact of wind-generated ocean waves upon the evolution of an idealized cyclone is investigated. Simulations are performed using initial conditions based on winter-mean climatology. Experiments were completed with a constant z_0, a z_0 from Charnock's relation, and a z_0 that includes wave-stress effects from the WAM model. Zonal SST and sinusoidal SST distributions were used.

The results indicate that for this set of initial conditions, the frictional effects of wind-generated ocean waves can influence the boundary-layer structure in the vicinity of a marine cyclone. Because of large near-surface wind speeds, substantial growth of surface ocean waves occurs with maximum significant wave heights in excess of 12 m. The wave height maxima occur along the warm front and to the rear of the cyclone where wind speeds are largest. However, because the translational speed of the cyclone approaches 20 m s^{-1}, at times, the winds are rapidly changing relative to the ocean surface. As a result, the ocean waves in these high wind speed regions are relatively young (growing) and the coupling between the atmospheric boundary layer and the ocean surface is large. In regions of high wind speeds, the Charnock formula appears to underestimate the surface roughness and momentum flux for young ocean waves. Comparison of the simulations suggest that the increased effective roughness associated with young ocean waves, increases the surface stress, decreases the lowest model level wind speeds by as much as 12% relative to the simulation that used the Charnock formula and by over 20% compared with the simulation that used a constant z_0. At times, the heat and moisture fluxes increase in the coupled simulations in the southwest quadrant by 30% relative to the simulation that used the Charnock formula and by 60% compared with the simulation that used a constant z_0. As a consequence of the young ocean waves, the localized regions of increased TKE (by up to 20% relative to CHZSST and 50% relative to ZSST) and eddy mixing coefficients result in increased vertical transport of heat, momentum and moisture.

The cyclone-scale and mesoscale structure of the simulated idealized cyclone is modified by effective roughness changes associated with ocean waves, as well. A comparison of the constant z_0 and coupled simulations indicates that the response of the central pressure of the idealized cyclone to the frictional changes associated with ocean waves is complex and can vary by as much as 10 mb. The differences in the central pressure between the model simulation that used the Charnock formula and the coupled simulation are up to 8 mb. The roughness effects of ocean waves appear, at times, to augment the filling of cyclones, which is often poorly simulated in operational and research numerical models. Additionally, the domain mean kinetic energy during rapid development is decreased substantially near the surface and up to 3–8% throughout the middle- and upper-troposphere relative to both the simulations that used constant z_0 and the Charnock formula. Mesoscale structures are modulated in regions where young waves exist. For example, the local pressure gradient near the cyclone center appears to be particularly sensitive to the roughness changes. Furthermore, young ocean waves act to increase the effective roughness to the rear of the cyclone, where the cold air mass is advected over the warm SSTs, and increase the rainfall rate (by over 34%, locally relative to CHZSST and by two-fold relative to ZSST) during the period of rapid development. The frontal strength in the lowest 1 km above the surface is intensified in localized regions along the warm and cold fronts.

5. Acknowledgments

The idea for this research was formulated after fruitful discussions with Melvyn Shapiro and Wendell Nuss. Peter Janssen and Paul Wittmann provided very beneficial background information concerning ocean wave modeling and the WAM model. Jack Kain graciously provided the code for the Kain-Fritsch convective parameterization scheme. Helpful discussions with Steve Burk, Richard Hodur, John Glendening, Jack Kain, William Thompson and Liana Zambresky also contributed to this work. This research was funded by the Naval Research Laboratory's Coastal Meteorology ARI PE-0601153N and the Office of Naval Research PE-0602704N. This work was supported in part by a grant of HPC time from the DoD Shared Resource Center, US Army Corps of Engineers Waterways Experiment Station HPC Center and performed on a Cray C-90.

REFERENCES

Anthes, R. A. and Keyser, D. 1979. Tests of a fine-mesh model over Europe and the United States. *Mon. Wea. Rev.* **107**, 963–984.

Bosart, L. F. 1981. The President's Day snowstorm of 18–19 February 1979. A subsynoptic-scale event. *Mon. Wea. Rev.* **109**, 1542–1566.

Brunt, D. 1930. The present position of theories of the origin of cyclonic depressions. *Quart. J. Roy. Meteor. Soc.* **56**, 345–350.

Charnock, H. 1955. Wind stress on a water surface. *Quart. J. Roy. Meteor. Soc.* **81**, 639–640.

Danard, M. B. 1969. Numerical studies of effects of surface friction on large-scale atmospheric motions. *Mon. Wea. Rev.* **97**, 835–844.

Danard, M. B. and Ellenton, G. E. 1980. Physical influences on East Coast Cyclogenesis. *Atmosphere: Atmos.-Ocean* **18**, 65–82.

Dolan, R. and Davis, R. E. 1992. Rating northeasters. *Marin. Wea. Log.* **36**, 4–11.

Doyle, J. D. and Warner, T. T. 1993. A numerical investigation of coastal frontogenesis and mesoscale cyclogenesis during GALE IOP 2. *Mon. Wea. Rev.* **121**, 1048–1077.

Graystone, P. 1962. The introduction of topographic and frictional effects in a baroclinic model. *Quart. J. Roy. Meteor. Soc.* **88**, 256–270.

Haar, P. A., Elsberry, R. L., Hogan, T. F. and Clune, W. M. 1992. Forecasts of north Pacific maritime cyclones with the Navy operational global atmospheric prediction system. *Wea. Forecasting* **7**, 456–467.

Hodur, R. M. 1993. *Development and testing of the coupled ocean/atmosphere mesoscale prediction system (COAMPS)*. NRL/MR/7533-93-7213, Naval Research Laboratory, 84 pp. (Available from Naval Research Laboratory, Monterey, CA 93943-5502.)

Hines, K. M. and Mechoso, C. R. 1993. Influence of surface drag on the evolution of fronts. *Mon. Wea. Rev.* **121**, 1152–1175.

Janssen, P. A. E. M. 1989. Wave-induced stress and the drag of air flow over sea waves. *J. Phys. Oceanogr.* **19**, 745–754.

Janssen, P. A. E. M. 1991. Quasi-linear theory of wind-wave generation applied to wave forecasting. *J. Phys. Oceanogr.* **21**, 1631–1642.

Janssen, P. A. E. M. 1994. *Results with a coupled wind wave model.* Technical Report no. 71. 60 pp. (Available from ECMWF, Shinfield Park, Reading RG2 9Ax, UK.)

Janssen, P. A. E. M., Lionello, P. and Zambresky, L. 1989. On the interaction of wind and waves. *Phil. Trans. R. Soc. London* **A329**, 289–301.

Juang, H.-M. and Ogura, Y. 1990. A case study of rapid cyclogenesis over Canada. Part II: Simulations. *Mon. Wea. Rev.* **118**, 674–704.

Kain, J. S. and Fritsch, J. M. 1990. A one-dimensional entraining/detraining plume model and its application in convective parameterization. *J. Atmos. Sci.* **47**, 2784–2802.

Komen, G. J. 1985. Energy and momentum fluxes through the sea surface. *Dynamics of the ocean surface mixed layer*, P. Muller and D. Henderson (eds.).

Proceedings 'Aha Hulika'a, Hawaii Institute of Geophysics, special publications, 1987, 207–217.

Kuo, Y.-H. and Reed, R. J. 1988. Numerical simulation of an explosively deepening cyclone in the Eastern Pacific. *Mon. Wea. Rev.* **116**, 2081–2105.

Kuo, Y.-H., Reed, R. J. and Low-Nam, S. 1991. Effects of surface energy fluxes during the early development and rapid intensification stages of seven explosive cyclones in the Western Atlantic. *Mon. Wea. Rev.* **119**, 457–476.

Lorenz, E. N. 1967. *The nature and theory of the general circulation of the atmosphere*. WMO Report, 218, 161 pp.

Louis, J. F., Tiedtke, M. and Geleyn, J. F. 1982. A short history of the operational PBL-parameterization at ECMWF. *Workshop on Planetary Boundary Parameterization, ECMWF, Reading*, 59–79. (Available from ECMWF, Shinfield Park, Reading RG2 9Ax, UK.)

Maat, N., Kraan, C. and Oost, W. A. 1991. The roughness of wind waves. *Bound.-Layer Meteor.* **54**, 89–103.

Neiman, P. J. and Shapiro, M. A. 1993. The life cycle of an extratropical marine cyclone. Part I: Frontal-cyclone evolution and thermodynamic air-sea interaction. *Mon. Wea. Rev.* **121**, 2153–2176.

Nordeng, T. E. 1991. On the wave age dependent drag coefficient and roughness length at sea. *J. Geophys. Res.* **96**, 7167–7174.

Nuss, W. A. and Anthes, R. A. 1987. A numerical investigation of low-level processes in rapid cyclogenesis. *Mon. Wea. Rev.* **115**, 2728–2743.

Oort, A. H. 1983. *Global atmospheric circulation statistics*, 1958–1973. NOAA Prof. Pap. 14, 180 pp. (NTIS PB84-129717.)

Petterssen, S., Bradbury, D. L. and Pedersen, K. 1962. The Norwegian cyclone models in relation to heat and cold sources. *Geofys. Publ.* **24**, 243–280.

Rutledge, S. A. and Hobbs, P. V. 1983. The mesoscale and microscale structure of organization of clouds and precipitation in midlatitude cyclones. VIII: A model for the "seeder-feeder" process in warm-frontal rainbands. *J. Atmos. Sci.* **40**, 1185–1206.

Sanders, F. and Gyakum, J. R. 1980. Synoptic-dynamic climatology of the "bomb". *Mon. Wea. Rev.* **108**, 1589–1606.

Smith, B. B. and Mullen, S. L. 1993. An evaluation of sea level cyclone forecasts produced by NMC's nested-grid model and global spectral model. *Wea. Forecasting* **8**, 37–56.

Smith, S. D., Anderson, R. J., Oost, W. A., Kraan, C., Maat, N., De Cosmo, J., Katsaros, K. B., Davidson, K., Bumke, K., Hasse, L. and Chadwick, H. M. 1992. Sea surface wind stress and drag coefficients. The HEXOS results. *Bound-layer Meteor.* **60**, 109–142.

Therry, G. and Lacarrére, P. 1983. Improving the eddy kinetic energy model for planetary boundary layer description. *Bound.-Layer Meteor.* **25**, 63–88.

Ulbrich, U., Burger, G., Schriever, D., Von Storch, H., Weber, S. L. and Schmitz, G. 1993. The effect of a regional increase in ocearn surface roughness on the tropospheric circulation, a GCM experiment. *Climate Dyn.* **8**, 277–285.

The WAMDI Group (S. Hasselmann, K. Hasselmann, E. Bauer, P. A. E. M. Janssen, G. Komen, L. Bertotti, P. Lionello, A. Guillaume, V. Cardone, J. Greenwood, M. Reistad, L. Zambresky and J. Ewing), 1988. The WAM model-a third generation ocean wave prediction model. *J. Phys. Oceanogr.* **18**, 1775–1810.

Weber, S. L. 1994. Statistics of the air-sea fluxes of momentum and mechanical energy in a coupled wave-atmosphere model. *J. Phys. Oceanogr.* **24**, 1388–1398.

Weber, S. L., Von Storch, H., Viterbo, P. and Zambresky, L. 1993. Coupling an ocean wave model to an atmospheric general circulation model. *Clim. Dyn.* **9**, 63–69.